Nonlinear dynamics of intense ion beam envelopes

Qian Qian and Ronald C. Davidson
Plasma Physics Laboratory, Princeton University, Princeton, New Jersey 08543
(Received 13 December 1995)

The nonlinear envelope equations for an intense Kapchinskij-Vladimirskij (KV) beam equilibrium are studied self-consistently for the case of a periodic quadrupole focusing lattice. First, the linearized solutions to the two nonlinearly coupled envelope equations for a matched KV beam are obtained in the smooth-beam approximation. A comparison between the solutions of the linearized equations and the (numerically solved) nonlinear equations is presented. Second, the nonlinear evolution of the envelopes for a mismatched beam is studied numerically. It is found that the oscillation of the beam envelope exhibits chaotic behavior in certain regions of the parameter space $(KS/\varepsilon,\sigma_v)$. Here, K is the self-field perveance, ε is the unnormalized beam emittance, S is the axial periodicity length, and J_v is the vacuum phase advance. Detailed numerical results are presented and the stable regime in the parameter space $(KS/\varepsilon,\sigma_v)$ is determined numerically. It is found that the threshold condition for the onset of unstable oscillations of the envelope functions is independent of the filling factor η of the quadrupole focusing lattice. [S1063-651X(96)08605-1]

PACS number(s): 07.77.−n, 29.27.Eg, 41.75.−i, 52.25.Wz

I. INTRODUCTION

Periodic focusing accelerators [1] have a wide range of applications ranging from scientific research to industrial processes [2–4]. There is growing interest in the physics of advanced high-current ion accelerators, particularly for applications such as heavy ion fusion [5,6] and nuclear waste treatment [7]. In these applications, the requirements of low cost and high efficiency are critical factors and must be met by optimizing aperture size and minimizing beam particle losses and beam envelope instabilities. One of the challenges of intense ion beam propagation relates to avoiding the effects of collective instabilities, which become important when space-charge effects are comparable to the external focusing force [8–17]. Electrostatic and electromagnetic instabilities due to various features of the beam distribution function in phase space place severe limits on the parameter regimes where a beam can be propagated stably with minimal loss of beam particles [1,3,4]. One important class of instabilities pertains to perturbations about the Kapchinskij-Vladimirskij (KV) beam distribution [18], which is the only known steady-state beam equilibrium $(\partial/\partial s=0)$ for beam propagation through an alternating-gradient focusing lattice with fully self-consistent space-charge effects. The KV distribution function is singular in phase space and is susceptible to various collective instabilities.

We consider here an infinitely long, intense ion beam propagating through an alternating-gradient quadrupole focusing lattice with periodicity length S in the axial direction (Fig. 1). In the laboratory frame, a fixed, right-handed Cartesian coordinate system (X,Y,Z) is employed, with the Z coordinate denoting the longitudinal direction. The quantities X and Y measure the transverse distances from the beam axis at $(X,Y)=(0,0)$. The axis of the beam transport system coincides with the ideal path of the beam particles for a thin beam with $a,b\ll S$, where a and b are the transverse beam dimensions in the X and Y directions, respectively. A similar Cartesian coordinate system (x,y,z) is established in the (moving) beam frame, with $(x,y)=(X,Y)$ and $z=Z-v_b t$, where v_b is the average axial velocity of the beam particles. Both coordinate systems are illustrated in Fig. 1. Following the standard convention in accelerator physics [1–3,19], the new independent variable $s=v_b t$ is introduced, corresponding to the axial displacement of a beam ion in the beam propagation direction.

For a KV beam equilibrium, the corresponding density profile in configuration space is uniform and equal to a constant value $\hat{n}_b$ within the elliptical cross section $x^2/a^2+y^2/b^2=1$ (Fig. 2). The beam boundary is defined by the two envelope functions $a(s)$ and $b(s)$ in the transverse plane (x,y). The envelope functions $a(s)$ and $b(s)$ satisfy the familiar nonlinear envelope equations [1,3,4,20]

$$\frac{d^2}{ds^2}a(s)+\kappa_q(s)a(s)-\frac{2K}{a(s)+b(s)}-\frac{\varepsilon_x^2}{a^3(s)}=0, \quad (1)$$

$$\frac{d^2}{ds^2}b(s)-\kappa_q(s)b(s)-\frac{2K}{a(s)+b(s)}-\frac{\varepsilon_y^2}{b^3(s)}=0. \quad (2)$$

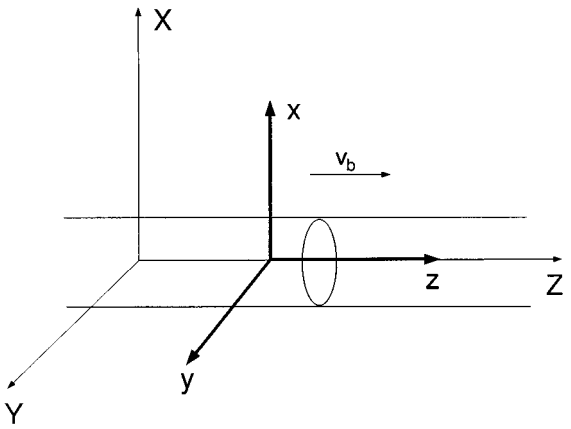

FIG. 1. Cartesian coordinate systems in the laboratory frame and in the frame of the beam moving with axial velocity v_b (the bold coordinate system).

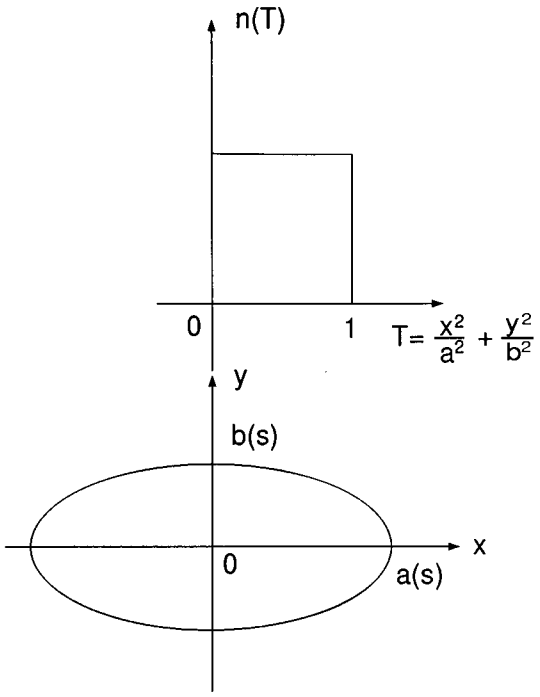

FIG. 2. Uniform density profile for a KV beam equilibrium with elliptical cross section.

In Eqs. (1) and (2), the quadrupole focusing terms are proportional to the lattice function $\kappa_q(s)$ defined by

$$\kappa_q(s)=\frac{ZeB_q'(s)}{\gamma_b m_i \beta_b c^2}. \tag{3}$$

For a periodic focusing lattice, which is the case considered here, the lattice function $\kappa_q(s)$ satisfies

$$\kappa_q(s+S)=\kappa_q(s), \tag{4}$$

where S is the axial periodicity length. The quadrupole focusing terms in Eqs. (1) and (2) are balanced by the repulsive terms proportional to the normalized beam emittances ε_x and ε_y and by the repulsive terms proportional to the self-field perveance K defined by

$$K=\frac{I_b}{(m_i c^2/Ze)}\frac{2}{\beta_b^3\gamma_b^3}. \tag{5}$$

Here m_i and Ze are the ion rest mass and charge, respectively, I_b is the beam current, $\beta_b c=v_b$ is the average axial velocity of the beam ions, $\gamma_b=(1-\beta_b^2)^{-1/2}$ is the relativistic mass factor, c is the speed of light *in vacuo*, and $B_q'(s)\equiv(\partial B_x^q/\partial y)_0=(\partial B_y^q/\partial x)_0$ is the quadrupole field gradient at the beam axis at $(x,y)=(0,0)$. The nonlinear evolution of the beam envelope functions $a(s)$ and $b(s)$ determines the confinement region of the beam particles within a KV beam equilibrium.

Note from Eqs. (1) and (2) that the envelope equations are nonlinearly coupled by the self-field terms proportional to K. Therefore, space-charge effects can play an important role in the nonlinear evolution of the envelope functions $a(s)$ and $b(s)$, particularly when the self-field perveance K is sufficiently large.

By solving the envelope equations (1) and (2), which are two nonlinearly coupled, second-order differential equations, the envelope functions for a KV beam with elliptical cross section can be obtained for a *matched* beam by imposing periodic boundary conditions [1,20]. Because a perfect matching of the beam envelope is difficult to achieve experimentally, it is of considerable practical importance to study the stability behavior of the beam envelope for the case of a slight mismatch, i.e., for small perturbations around the equilibrium matched solution. Previously, linear stability analyses of the envelope equations (1) and (2) have been carried out, indicating the presence of linear instabilities in certain regimes of parameter space [11,12]. However, the fully nonlinear evolution of the beam envelope has not heretofore been investigated systematically. Two consequences of beam envelope instabilities include beam particle loss and emittance growth. In this paper, the nonlinear envelope equations (1) and (2), including self-consistent space-charge effects, are investigated numerically. This work not only confirms earlier linear results, but also reveals new nonlinear phenomena important in the evolution of the beam envelope, including chaotic behavior and the nonlinear saturation of linear instabilities.

In Sec. II, for a matched beam, the linearized solutions to the envelope equations are obtained in the smooth-beam approximation and these solutions are compared with the (exact) numerical results for various choices of system parameters. In Sec. III, for a mismatched beam, the nonlinear evolution of the envelope functions is investigated and the stability regime in the parameter space $(KS/\varepsilon,\sigma_v)$ is determined numerically, where the quantity σ_v is the vacuum phase advance defined in Eq. (21). Finally, conclusions are summarized in Sec. IV.

II. ENVELOPE SOLUTION FOR A MATCHED BEAM

Based upon the envelope equations (1) and (2) for a KV beam equilibrium, the evolution of the envelope functions $a(s)$ and $b(s)$ is investigated for the cases of a matched beam (this section) and a mismatched beam (Sec. III). In both cases, the (unnormalized) rms emittances ε_x and ε_y in Eqs. (1) and (2) are assumed to be constant.

For a matched KV beam, the nonlinearly coupled envelope equations (1) and (2) can be solved numerically [21], with the periodic boundary conditions

$$a(s+S)=a(s), \quad b(s+S)=b(s), \tag{6}$$

for a variety of system parameters, whereas the analytical solutions to the KV envelope equations are generally difficult to obtain. In addition, the numerically determined nonlinear solutions for the envelope functions $a(s)$ and $b(s)$ can be used to obtain *exact* estimates for the phase advances σ_x and σ_y, defined by

$$\sigma_x=\varepsilon_x\int_{s_0}^{s_0+S}\frac{ds}{a^2(s)}, \quad \sigma_y=\varepsilon_y\int_{s_0}^{s_0+S}\frac{ds}{b^2(s)}. \tag{7}$$

For isotropic beam emittance with $\varepsilon_x=\varepsilon_y\equiv\varepsilon$, it is found that $\sigma_x=\sigma_y=\sigma$, where

$$\sigma=\varepsilon\int_{s_0}^{s_0+S}\frac{ds}{a^2(s)}=\varepsilon\int_{s_0}^{s_0+S}\frac{ds}{b^2(s)}. \tag{8}$$

In the *smooth-beam* approximation, where the envelope oscillations are assumed to be small amplitude, the envelope equations (1) and (2) can be solved approximately by the linearization approximation. It was shown in a previous calculation [21] that, when the envelope functions $a(s)$ and $b(s)$ undergo *small-amplitude* oscillations about the constant average values $\overline{a}$ and $\overline{b}$, the linear solution to the envelope functions can be expressed in the Fourier series representations

$$a(s)=\overline{a}+\delta a(s)=\overline{a}+\sum_{-\infty}^{\infty}\delta a_n\exp(ik_ns), \tag{9}$$

$$b(s)=\overline{b}+\delta b(s)=\overline{b}+\sum_{-\infty}^{\infty}\delta b_n\exp(ik_ns). \tag{10}$$

Here the quantities $\overline{a}$, $\overline{b}$, δa_n, and δb_n are determined from [21]

$$\frac{2K}{\overline{a}+\overline{b}}+\frac{\varepsilon_x^2}{\overline{a}^3}=\sum_{n=-\infty}^{\infty}\kappa_n^2\frac{\overline{b}\lambda+[\lambda+3\varepsilon_y^2/\overline{b}^4-k_n^2]\overline{a}}{\lambda^2-[\lambda+3\varepsilon_x^2/\overline{a}^4-k_n^2][\lambda+3\varepsilon_y^2/\overline{b}^4-k_n^2]}, \tag{11}$$

$$\frac{2K}{\overline{a}+\overline{b}}+\frac{\varepsilon_y^2}{\overline{b}^3}=\sum_{n=-\infty}^{\infty}\kappa_n^2\frac{\overline{a}\lambda+[\lambda+3\varepsilon_x^2/\overline{a}^4-k_n^2]\overline{b}}{\lambda^2-[\lambda+3\varepsilon_x^2/\overline{a}^4-k_n^2][\lambda+3\varepsilon_y^2/\overline{b}^4-k_n^2]}, \tag{12}$$

$$\delta a_n=\kappa_n\frac{\lambda\overline{b}+[\lambda+3\varepsilon_y^2/\overline{b}^4-k_n^2]\overline{a}}{\lambda^2-[\lambda+3\varepsilon_x^2/\overline{a}^4-k_n^2][\lambda+3\varepsilon_y^2/\overline{b}^4-k_n^2]}, \tag{13}$$

$$\delta b_n=-\kappa_n\frac{\overline{a}\lambda+[\lambda+3\varepsilon_x^2/\overline{a}^4-k_n^2]\overline{b}}{\lambda^2-[\lambda+3\varepsilon_x^2/\overline{a}^4-k_n^2][\lambda+3\varepsilon_y^2/\overline{b}^4-k_n^2]}. \tag{14}$$

In Eqs. (9)–(14), the quantities κ_n, k_n, and λ are defined by

$$\kappa_n=\frac{1}{S}\int_{s_0}^{s_0+S}ds\,\kappa_q(s)\exp(-ik_ns), \tag{15}$$

$$k_n=\frac{2\pi n}{S}\quad(n=0,\pm1,\pm2,\ldots), \tag{16}$$

$$\lambda=\frac{2K}{(\overline{a}+\overline{b})^2}. \tag{17}$$

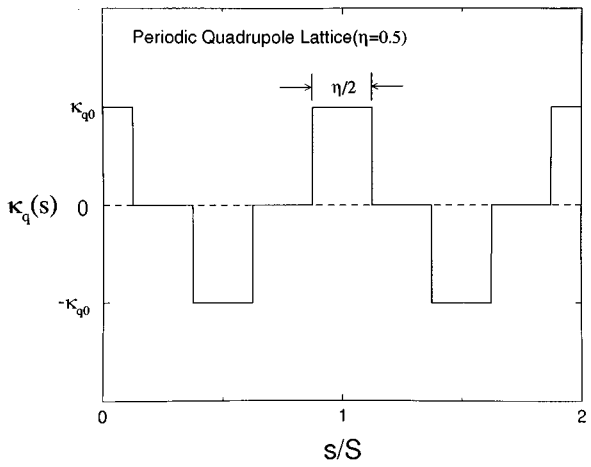

FIG. 3. Lattice function $\kappa_q(s)$ for an alternating-gradient quadrupole magnetic field with periodic step-function profile and filling factor $\eta=0.5$.

Equations (11) and (12) are nonlinearly coupled transcendental equations for the average envelopes $\overline{a}$ and $\overline{b}$ and are applicable for a wide range of choices of periodic lattice function $\kappa_q(s)$ that satisfy $\kappa_q(s+S)=\kappa_q(s)$ and $\kappa_q(-s)=\kappa_q(s)$. For the special case of a symmetric beam with equal emittances in the x and y directions, i.e., $\varepsilon_x=\varepsilon_y\equiv\varepsilon$, Eqs. (11) and (12) reduce to

$$\frac{\varepsilon^2}{r_b^3}+\frac{K}{r_b}=\sum_{n=-\infty}^{\infty}\frac{\kappa_n^2r_b}{k_n^2-3\varepsilon^2/r_b^4}, \tag{18}$$

whereas Eqs. (13) and (14) reduce to

$$\delta a_n=-\delta b_n=\frac{\kappa_nr_b}{k_n^2-3\varepsilon^2/r_b^4}, \tag{19}$$

where $r_b=\overline{a}=\overline{b}$. Equation (18) can be solved for any specified periodic lattice function $\kappa_q(s)$ to obtain the average beam radius r_b, whereas $\delta a(s)$ and $\delta b(s)$ can be estimated from Eqs. (9), (10), and (19).

Throughout the remainder of this paper we consider the case where the beam propagates through the periodic step-function lattice defined by (Fig. 3)

$$\kappa_q(s)=\begin{cases}+\hat{\kappa}_q, & 0\leqslant s<(\eta/2)S/2\\ 0, & (\eta/2)S/2\leqslant s<(1-\eta/2)S/2\\ -\hat{\kappa}_q, & (1-\eta/2)S/2\leqslant s<(1+\eta/2)S/2\\ 0, & (1+\eta/2)S/2\leqslant s<(2-\eta/2)S/2\\ +\hat{\kappa}_q, & (2-\eta/2)S/2\leqslant s<S,\end{cases} \tag{20}$$

where η is the filling factor and $\hat{\kappa}_q$ is the amplitude of the lattice function. For future reference, it is convenient to measure the strength of the quadrupole focusing field in terms of the vacuum phase advance σ_v defined in the limit of negligibly small beam intensity K by

$$\sigma_v=\lim_{K\to0}\varepsilon\int_{s_0}^{s_0+S}\frac{ds}{a^2(s)}, \tag{21}$$

where $\varepsilon_x=\varepsilon_y=\varepsilon$ is assumed. Making use of the matrix method [4], a careful examination of Eqs. (1) and (2) for $K\to 0$ shows that σ_v is determined exactly for the case of the periodic step-function lattice in Eq. (20) by [4]

$$\cos\sigma_v=\cosh\varphi_1(\cos\varphi_1-\varphi_2\sin\varphi_1)+\varphi_2\sinh\varphi_1(\cos\varphi_1-\tfrac{1}{2}\varphi_2\sin\varphi_1). \tag{22}$$

Here the quantities φ_1 and φ_2 are defined by

$$\varphi_1\equiv\tfrac{1}{2}\sqrt{\hat{\kappa}_q}\,\eta S,$$

$$\varphi_2\equiv\tfrac{1}{2}\sqrt{\hat{\kappa}_q}(1-\eta)S=\frac{1-\eta}{\eta}\,\varphi_1. \tag{23}$$

Therefore, a specification of η and $\sqrt{\hat{\kappa}_q}S$ permits an exact determination of the vacuum phase advance σ_v from Eq. (22), which is valid in the limit of negligibly small beam intensity with $K\to 0$. In previous calculations by the authors (see, for example, Ref. [21]), we made use of the quadratic measure, denoted by σ_0, of the strength of the periodic focussing field defined by

$$\frac{\sigma_0^2}{S^2}\equiv\int_{s_0}^{s_0+S}\frac{ds}{S}\left(\int_{s_0}^{s_0+s}ds'\,\kappa_q(s')\right)^2=\sum_{n=1}^{\infty}\frac{2\kappa_n^2S^2}{(2\pi n)^2}=\tfrac{1}{16}\hat{\kappa}_q^2S^2\eta^2(1-\tfrac{2}{3}\eta). \tag{24}$$

Comparing Eqs. (23) and (24), we note that σ_0 and φ_1 are related by $\sigma_0^2=\varphi_1^4(1-2\eta/3)/\eta^2$. For sufficiently weak focusing field amplitude ($\varphi_1\ll\pi/2$), it can be shown from the exact expression for $\cos\sigma_v$ in Eq. (22) that $\sigma_v\simeq\sigma_0$, where σ_0 is defined in Eq. (24). However, except for small values of σ_v, the quantity σ_0 consistently gives an underestimate of the exact vacuum phase advance σ_v determined from Eq. (22). This is evident from Fig. 4, where σ_v/σ_0 is plotted versus σ_v for three values of η corresponding to $\eta=0.3,0.5,0.7$.

Of course, as the beam intensity K is increased, the actual advance σ, defined in Eq. (8) and determined numerically from the nonlinear envelope equations (1) and (2), is *depressed* relative to the vacuum value σ_v defined in Eq. (21) for $K\to 0$. This is illustrated in Fig. 5, where σ/σ_v is plotted versus the normalized self-field perveance KS/ε for the case where $\sigma_v=60°$, $\eta=0.5$, and $\varepsilon_x=\varepsilon_y=\varepsilon$.

Shown in Fig. 6 is a plot of the periodic envelope functions $a(s+S)=a(s)$ and $b(s+S)=b(s)$ for a matched beam propagating through the periodic step-function lattice defined in Eq. (20). The numerical solutions to the exact nonlinear envelope equations (1) and (2) are shown by the solid curves in Fig. 6, whereas the analytical estimates obtained in the smooth-beam approximation for small-amplitude envelope oscillations about the average radius $\overline{a}=b$ are shown by the dashed curves. The choice of system parameters in Fig. 6 corresponds to $\eta=0.5$, $\sigma_v=63°$, $KS/\varepsilon_x=2$, $\sigma=27.7°$, and $\varepsilon_x=\varepsilon_y$. In Fig. 6 the envelope functions $a(s)$ and $b(s)$ are plotted in terms of the rescaled quantities $a(s)/\sqrt{\varepsilon S}$ and $b(s)/\sqrt{\varepsilon S}$, respectively. It is evident from Fig. 6 that the linear solution to the envelope equations is an excellent approximation to the exact solution for the choice of system parameters in the figure.

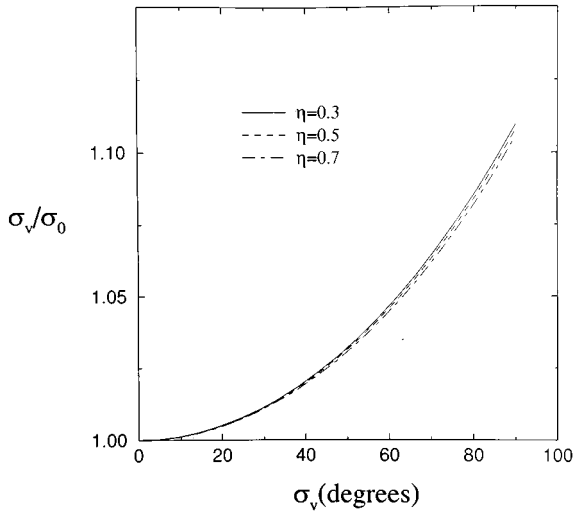

FIG. 4. Plot of σ_v/σ_0 versus the vacuum phase advance σ_v for $\varepsilon_x=\varepsilon_y=\varepsilon$ and three values of filling factor $\eta=0.3,0.5,0.7$. Here σ_v and σ_0 are defined in Eqs. (21) and (24).

To determine the parameter regime where the smooth-beam approximation is valid, a detailed comparison between the analytical estimate and the exact solution to Eqs. (1) and (2) is shown in Fig. 7. Here $r_b\equiv\overline{a}=b$ and $\delta r\equiv|\delta a(s)|_{\max}=|\delta b(s)|_{\max}$ are plotted versus the normalized self-field perveance KS/ε for the case of a step-function lattice with filling factor $\eta=0.5$ and several values of σ_v ranging from $\sigma_v=30°$ to 85°. In Fig. 7 the analytical estimates obtained in the smooth-beam approximation are plotted as solid curves, whereas the numerical results obtained from the

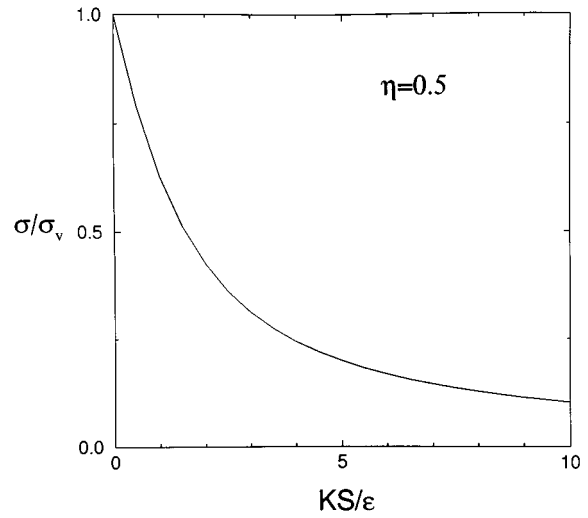

FIG. 5. Plot of σ/σ_v versus the normalized self-field perveance KS/ε for the choice of system parameters $\sigma_v=60°$, $\eta=0.5$, and $\varepsilon_x=\varepsilon_y=\varepsilon$. Here σ_v is defined in Eq. (21) and the phase advance σ is determined from Eq. (8) and the numerical solutions to the nonlinear envelope equations (1) and (2).

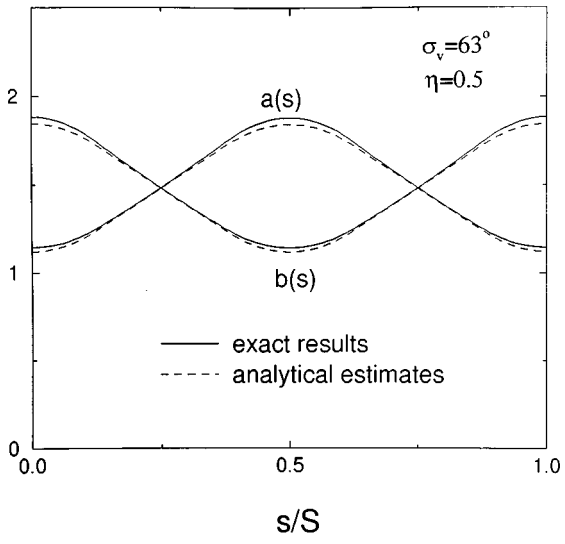

FIG. 6. Plot of the periodic envelope functions $a(s)$ and $b(s)$ of a matched beam propagating through a step-function lattice. The system parameters are specified by $\eta=0.5$, $\sigma_v=63°$, $KS/\varepsilon_x=2$, $\sigma=27.7°$, and $\varepsilon_x=\varepsilon_y$. The solid curves are numerical results obtained from the exact envelope equations, whereas the dashed curves correspond to the linear solutions obtained analytically in the smooth-beam approximation. Here $a(s)$ and $b(s)$ are plotted in terms of the rescaled quantities $a(s)/\sqrt{\varepsilon_x S}$ and $b(s)/\sqrt{\varepsilon_y S}$.

exact nonlinear solutions to the envelope equations (1) and (2) are plotted as dashed curves.

Figure 7(a) shows a plot of the average value of the envelope radius r_b. It is evident from Fig. 7(a) that the average radius r_b increases with increasing normalized self-field perveance KS/ε and decreases with increasing average focusing field as measured by σ_v. Note that the analytical estimate of the average beam radius obtained in the smooth-beam approximation provides an excellent approximation to the exact value of r_b calculated numerically from Eqs. (1) and (2).

A plot of the oscillation amplitude δr is shown in Fig. 7(b). Three points are noteworthy from Fig. 7(b). First, the oscillation amplitude of the envelope function δr increases with increasing σ_v and with increasing beam intensity as measured by KS/ε. Second, δr is different for different values of σ_v and the difference decreases with increasing KS/ε. Third, the analytical estimate of δr provides a good approximation to the exact result for values of σ_v in the range $\sigma_v \lesssim 60°$.

In conclusion, the KV envelope equations (1) and (2) have been solved in the smooth-beam approximation. The analytical estimate of the envelope functions provides an excellent approximation in the range $\sigma_v \lesssim 60°$ and in the large KS/ε limit. Because the rms envelope equations are identical to the KV envelope equations (1) and (2) [22], they can be solved in an identical manner in the smooth-beam approximation to that shown in this section, provided that the rms emittances ε_x and ε_y are approximately constant during the course of the beam propagation.

III. NONLINEAR EVOLUTION FOR A MISMATCHED BEAM

Perfect beam matching, where the envelope functions $a(s)$ and $b(s)$ precisely satisfy the periodic boundary condi-

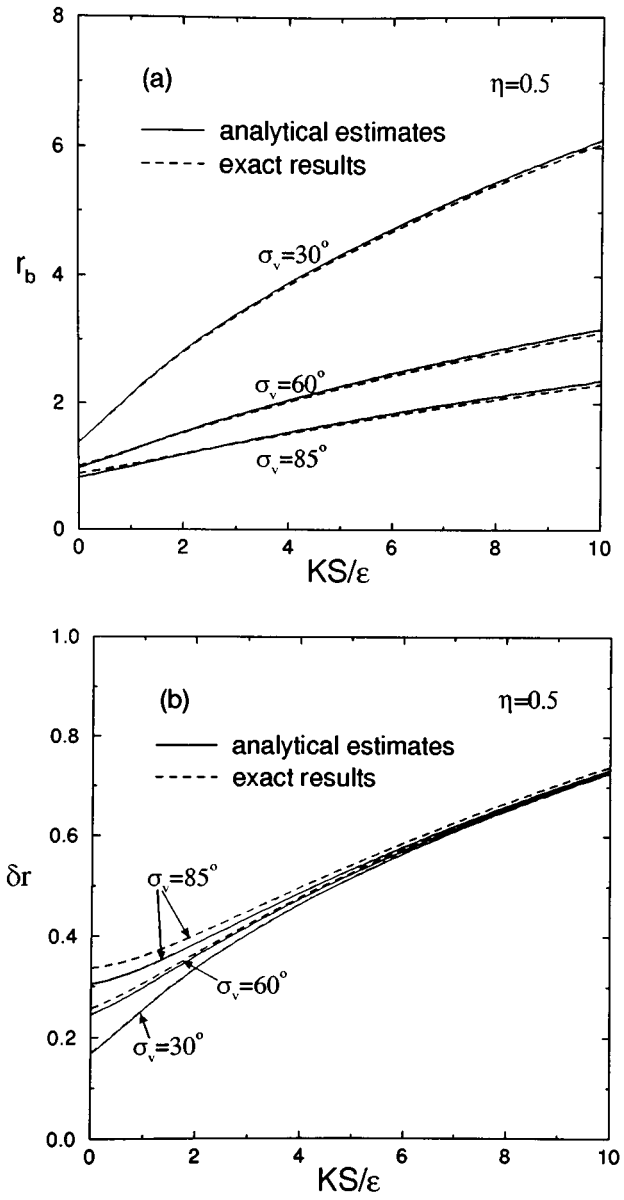

FIG. 7. Plots of the solutions for the envelope functions versus the normalized self-field perveance KS/ε for the case of a matched beam propagating through a step-function lattice with $\eta=0.5$ and $\sigma_v=30°$, 60°, and 85°. The two plots correspond to (a) the average value $r_b \equiv \overline{a}=\overline{b}$ and (b) the oscillating amplitude of the envelope functions $\delta r \equiv |\delta a(s)|_{\max}=|\delta b(s)|_{\max}$. The dashed curves correspond to the exact results, whereas the solid curves correspond to the analytical estimates obtained in the smooth-beam approximation. Here r_b and δr are plotted in terms of the rescaled quantities $r_b/\sqrt{\varepsilon S}$ and $\delta r/\sqrt{\varepsilon S}$, respectively.

tions in Eq. (6), is difficult to achieve in practical applications due to the various perturbations that affect the beam envelope. Therefore, it is of considerable practical importance to study the stability property of the envelope equations (1) and (2), because unstable oscillation of the envelope functions $a(s)$ and $b(s)$ can lead to beam particle losses. When the envelope functions $a(s)$ and $b(s)$ are perturbed about the equilibrium matched-beam solutions, the beam is said to be *mismatched.* The associated nonlinearity and the choice of system parameters $(KS/\varepsilon, \sigma_v)$ render the evolution

of $a(s)$ and $b(s)$ very complicated. Previous studies using a linearized model indicate that instabilities can exist in certain parameter regimes for the case of a mismatched beam [11,13]. The self-consistent, nonlinear evolution of the envelope functions has yet to be investigated for the case of a mismatched beam and is the subject of the analysis in this section.

To investigate the nonlinear evolution of the envelope functions $a(s)$ and $b(s)$, the envelope equations (1) and (2) are studied numerically. For purposes of illustration, a symmetric beam with $\varepsilon \equiv \varepsilon_x = \varepsilon_y$ is assumed to propagate through the step-function lattice shown in Fig. 3. To simplify the numerical analysis, the envelope equations are expressed in the dimensionless form

$$\frac{d^2}{d\hat{s}^2}\hat{a}(\hat{s}) + \hat{\kappa}_q(\hat{s})\hat{a}(\hat{s}) - \frac{2\hat{K}}{\hat{a}(\hat{s})+\hat{b}(\hat{s})} - \frac{1}{\hat{a}^3(s)} = 0, \quad (25)$$

$$\frac{d^2}{d\hat{s}^2}\hat{b}(\hat{s}) - \hat{\kappa}_q(\hat{s})\hat{b}(\hat{s}) - \frac{2\hat{K}}{\hat{a}(\hat{s})+\hat{b}(\hat{s})} - \frac{1}{\hat{b}^3(s)} = 0. \quad (26)$$

Here the dimensionless variables are defined by

$$\hat{s} = \frac{s}{S}, \quad \hat{a} = \frac{a}{\sqrt{\varepsilon S}}, \quad \hat{b} = \frac{b}{\sqrt{\varepsilon S}}, \quad \hat{\kappa}_q = \kappa_q S^2, \quad \hat{K} = \frac{KS}{\varepsilon}. \quad (27)$$

Equations (25) and (26) are characterized by two dimensionless parameters KS/ε and σ_v, where the quantity σ_v is determined in Eq. (22) for the case of a step-function lattice.

For a mismatched beam, Eqs. (25) and (26) constitute an initial-value problem without periodic boundary conditions. The beam is initially injected at $s=0$, the beginning of the focusing lattice shown in Fig. 3. The initial conditions for $a(s)$ and $b(s)$ at $s=0$ are chosen to be

$$a(0) = a_0(1+\Delta_x), \quad b(0) = b_0(1+\Delta_y), \quad (28)$$

where a_0 and b_0 are the matched-beam solutions at $s=0$. In Eq. (28), the initial mismatches Δ_x and Δ_y are taken to be in the range $0<|\Delta_x|<0.01$ and $0<|\Delta_y|<0.01$, respectively. The envelope equations (25) and (26) are integrated numerically for the choice of initial condition in Eq. (28). The solutions in the phase space (a,b,a',b') are plotted at the end of each lattice period, i.e., $s=0,S,2S,\ldots,NS$. Here $a' \equiv da/ds$ and $b' \equiv db/ds$. For present purposes, it is sufficient to study the Poincaré surface-of-section plot projected in the phase plane (a,a'), because the Poincaré surface-of-section plot projected onto the phase plane (b,b') is similar to that for the phase plane (a,a').

Figure 8 shows the Poincaré surface-of-section plots in the phase plane (a,a') for the case of a mismatched beam propagating through a step-function lattice with filling factor $\eta=0.5$ and vacuum phase advance $\sigma_v=63°$. The envelope function $a(s)$ has been followed for 1000 lattice periods ($s=1000S$). In Fig. 8, four plots are shown for different values of the normalized self-field perveance KS/ε corresponding to (a) $KS/\varepsilon=0.1$, $\sigma=60.2°$; (b) $KS/\varepsilon=1$, $\sigma=40.47°$; (c) $KS/\varepsilon=5$, $\sigma=13.14°$; and (d) $KS/\varepsilon=10$, $\sigma=6.8°$. It is evident from Figs. 8(a)–8(d) that the envelope function $a(s)$ is stable for small but finite perturbations about the matched-beam equilibrium. The evolution of $a(s)$ is regular and localized in the phase plane (a,a'). As a consequence, the beam is well confined for finite mismatch. In Fig. 8 and in all subsequent figures, the envelope function $a(s)$ is plotted in terms of the dimensionless quantity $a/\sqrt{\varepsilon S}$ as defined in Eq. (27), whereas the variable $a'=da/ds$ is scaled by the factor $\sqrt{S/\varepsilon}$.

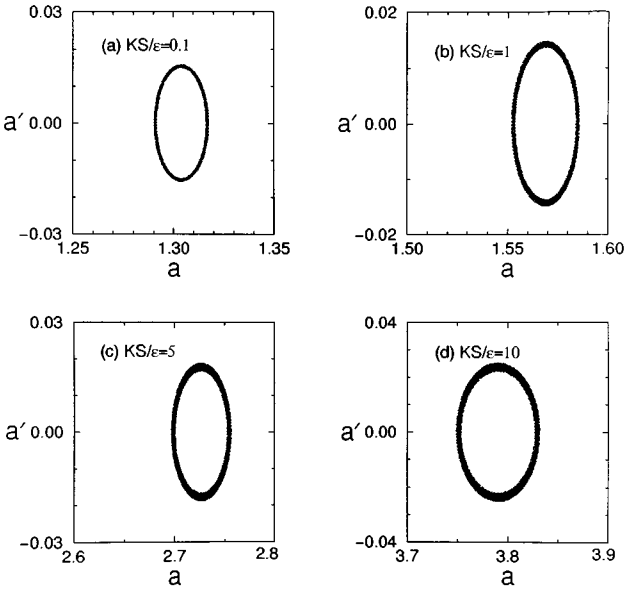

FIG. 8. Poincaré surface-of-section plots in the phase plane (a,a') for the case of a step-function lattice with filling factor $\eta=0.5$, vacuum phase advance $\sigma_v=63°$, and several values of the normalized self-field perveance KS/ε corresponding to (a) $KS/\varepsilon=0.1$, $\sigma=60.2°$; (b) $KS/\varepsilon=1$, $\sigma=40.47°$; (c) $KS/\varepsilon=5$, $\sigma=13.14°$; and (d) $KS/\varepsilon=10$, $\sigma=6.8°$. The evolution of the envelope function $a(s)$ has been followed for 1000 lattice periods.

Figure 9 shows numerical results obtained for the case of a mismatched beam for a larger value of vacuum phase advance σ_v, i.e., $\sigma_v=104°$. The Poincaré surface-of-section plots in the phase plane (a,a') are shown for different values of the normalized self-field perveance KS/ε corresponding to (a) $KS/\varepsilon=0.1$, $\sigma=102°$; (b) $KS/\varepsilon=0.6$, $\sigma=88.5°$; (c) $KS/\varepsilon=0.7$, $\sigma=86°$; (d) $KS/\varepsilon=1.5$, $\sigma=69°$; (e) $KS/\varepsilon=1.9$, $\sigma=62°$; and (f) $KS/\varepsilon=10$, $\sigma=17°$. The envelope function $a(s)$ has been followed for 1000 lattice periods ($s=1000S$). It is readily seen from Fig. 9 that there are two regimes where the envelope function $a(s)$ is stable, namely, $0 \leqslant KS/\varepsilon \lesssim 0.6$ and $KS/\varepsilon \geqslant 1.9$. The unstable regime corresponds to the range $0.6 \lesssim KS/\varepsilon \lesssim 1.9$. When the normalized self-field perveance KS/ε is larger than the threshold value $(KS/\varepsilon)_c \simeq 0.6$, the envelope function $a(s)$ exhibits bifurcation and the chaotic behavior evident in Figs. 9(c) and 9(d). Figure 10 shows the evolution of the unstable oscillation of the envelope function $a(s)$ for system parameters corresponding to those in Fig. 9(d). It is evident that the amplitude of the envelope oscillation grows nonlinearly. The corresponding chaotic motion of $a(s)$, in contrast to the regular motion in Fig. 8, leads to unstable, large-amplitude oscillations, which may ultimately result in beam particle losses.

To determine the parameter regime $(KS/\varepsilon, \sigma_v)$, where the envelope functions $a(s)$ and $b(s)$ are unstable, the envelope

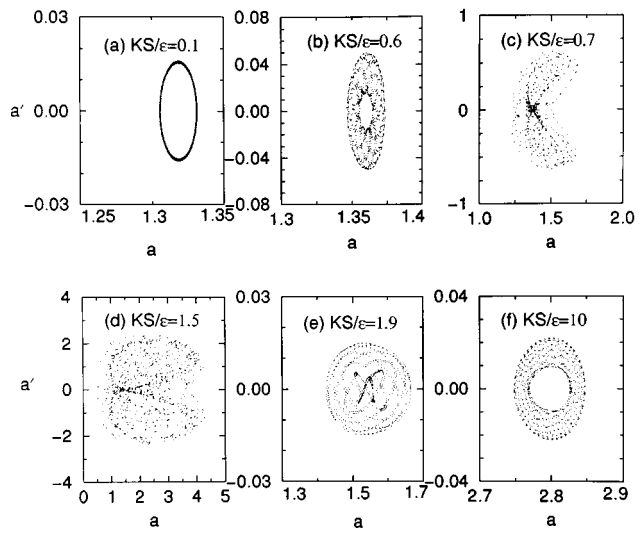

FIG. 9. Poincaré surface-of-section plots in the phase plane (a,a') for the case of a step-function lattice with filling factor $\eta=0.5$, vacuum phase advance $\sigma_v=104°$, and different values of the normalized self-field perveance KS/ε corresponding to (a) $KS/\varepsilon=0.1$, $\sigma=102°$; (b) $KS/\varepsilon=0.6$, $\sigma=88.5°$; (c) $KS/\varepsilon=0.7$, $\sigma=86°$; (d) $KS/\varepsilon=1.5$, $\sigma=69°$; (e) $KS/\varepsilon=1.9$, $\sigma=62°$; and (f) $KS/\varepsilon=10$, $\sigma=17°$. The evolution of the envelope function $a(s)$ has been followed for 1000 lattice periods.

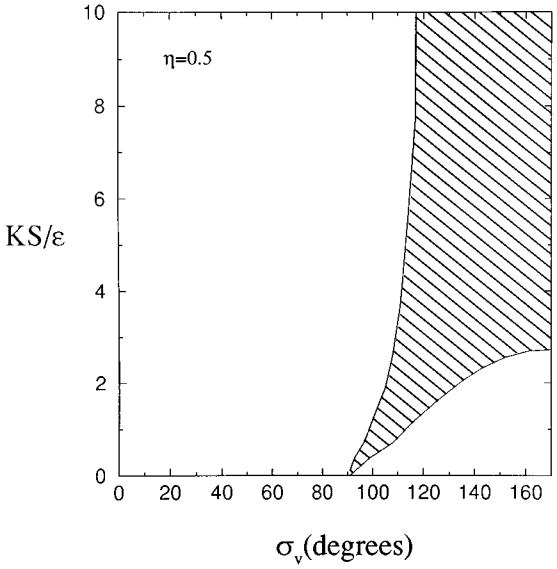

FIG. 11. Plot of the threshold value of KS/ε versus σ_v for the onset of chaotic behavior in the envelope function $a(s)$ for the case of a mismatched beam propagating through a step-function lattice with filling factor $\eta=0.5$. The unshaded areas are the stable regimes, whereas the shaded area is the unstable regime.

equations (25) and (26) have been integrated numerically for various choices of system parameters KS/ε and σ_v. The results are shown in Fig. 11, where the threshold value of KS/ε is plotted versus σ_v for the onset of chaotic behavior in the envelope function $a(s)$ as shown in Figs. 9(c) and 9(d). In the stable regimes (unshaded areas in Fig. 11) of the parameter space $(KS/\varepsilon,\sigma_v)$, the envelope functions $a(s)$ and $b(s)$ exhibit regular oscillations with small deviations from the matched-beam solution as shown in Fig. 8. In the unstable parameter regime (shaded area in Fig. 11), $a(s)$ and $b(s)$ exhibit chaotic behavior with large-amplitude oscillations. The result shown in Fig. 11 is found to be qualitatively consistent with the results obtained in previous studies using the Vlasov-Poisson equations [11,15].

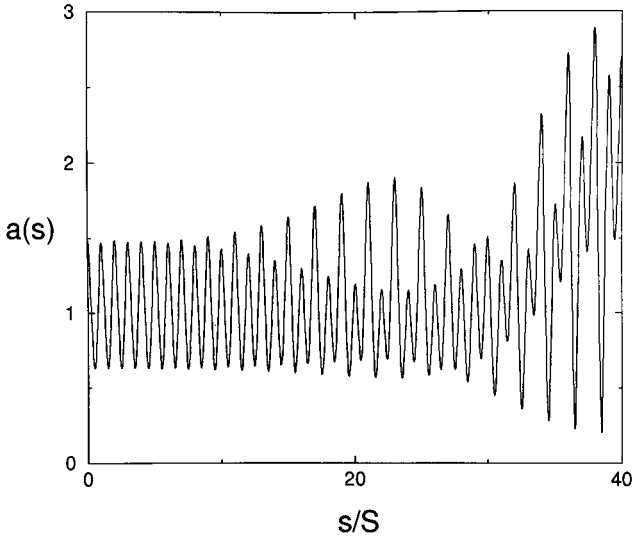

FIG. 10. Unstable oscillation of the envelope function $a(s)$ for system parameters corresponding to those in Fig. 9(d).

It is evident from Fig. 9 that the nonlinear evolution of the envelope function $a(s)$ for the case of a mismatched beam is related to the stability of the matched-beam solution to the envelope equations (25) and (26). The matched-beam solution to the envelope equations corresponds to the equilibrium position on the axis $a'=0$ in the phase plane (a,a'). In the stable region in the parameter space $(KS/\varepsilon,\sigma_v)$, the equilibrium position of $a(s)$ on the $a'=0$ axis is a (stable) O point in the phase space (a,a') as evident from Figs. 9(a), 9(b), 9(e), and 9(f). However, when the value KS/ε is in the unstable region, as shown in Figs. 9(c) and 9(d), the equilibrium position becomes an (unstable) X point. This indicates that the chaotic behavior of $a(s)$ for the case of a mismatched beam is related to the instability of the matched-beam solution to the envelope equations.

It is important to note that the features shown in Figs. 8 and 9 remain qualitatively similar for the nonlinear evolution of the envelope functions $a(s)$ and $b(s)$ when the filling factor η varies in the range $0<\eta<1$ for a wide range of choices of system parameters σ_v and KS/ε. In Fig. 12, the Poincaré surface-of-section plots are shown for the case of unstable oscillations of the envelope function $a(s)$ with different values of filling factor η corresponding to (a) $\eta=0.1$, (b) $\eta=0.3$, (c) $\eta=0.5$, and (d) $\eta=0.7$. Other system parameters have been chosen to be $\sigma_v=94°$, $KS/\varepsilon=0.3°$, $\sigma=85.7°$, and the envelope function $a(s)$ has been determined numerically for propagation over 1000 lattice periods. It is readily seen from Fig. 12 that the qualitative features of the unstable oscillations of the envelope function $a(s)$ remain the same for different filling factors η of the step-function lattice. It is further found that the threshold for the onset of unstable

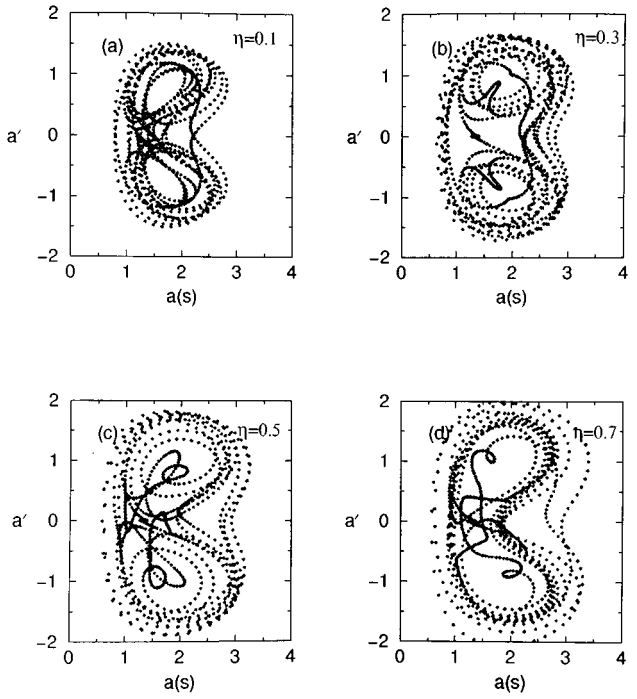

FIG. 12. Poincaré surface-of-section plots in the phase plane (a,a') for the case of a step-function lattice with $\sigma_v=94°$, $KS/\varepsilon=0.3$, $\sigma=85.7°$, and different values of the filling factor η corresponding to (a) $\eta=0.1$, (b) $\eta=0.3$, (c) $\eta=0.5$, and (d) $\eta=0.7$. The evolution of the envelope function $a(s)$ has been followed for 1000 lattice periods.

envelope oscillations does not depend upon the filling factor η. Therefore, it is concluded that the instability threshold in the parameter space $(KS/\varepsilon,\sigma_v)$, obtained for $\eta=0.5$ in Fig. 11, is also applicable for filling factors η in the range $0<\eta<1$.

IV. SUMMARY

In this paper, the nonlinear evolution of the beam envelope functions $a(s)$ and $b(s)$ has been investigated for the case of a uniform density KV beam. For the matched-beam case, it is found that the linearized solutions to the envelope equations are good approximations to the exact solutions in the parameter regime where the smooth-beam approximation is valid. For the mismatched-beam case, the evolution of the envelope functions is found to be complicated due to the nonlinear self-field effects in the envelope equations (1) and (2). The beam envelope function exhibits nonlinear instabilities when the average focusing field strength, as measured by σ_v, is sufficiently large. In the stable regime of the parameter space $(KS/\varepsilon,\sigma_v)$, it is found that the envelope functions $a(s)$ and $b(s)$ undergo regular, small-amplitude oscillations. In the unstable regime, it is found that $a(s)$ and $b(s)$ exhibit chaotic behavior with large oscillation amplitudes. Chaotic evolution of the beam envelope can lead to poor confinement of the beam particles and limit the allowed regime of parameter space $(KS/\varepsilon,\sigma_v)$ for stable beam propagation. The stable regime in the parameter space $(KS/\varepsilon,\sigma_v)$ has been determined numerically. Furthermore, the instability threshold in the parameter space $(KS/\varepsilon,\sigma_v)$ has been found to be independent of the filling factor η of the step-function focusing lattice.

ACKNOWLEDGMENTS

It is a pleasure to acknowledge the benefit of useful discussions with Chiping Chen. This research was supported in part by the U.S. Department of Energy Contract No. DE-AC02-76-CHO-3073 and in part by the Office of Naval Research.

[1] R. C. Davidson, *Physics of Nonneutral Plasmas* (Addison-Wesley, Reading, MA, 1990), Chap. 10, and references therein.
[2] D. A. Edwards and M. J. Syphers, *An Introduction to the Physics of High Energy Accelerators* (Wiley, New York, 1993).
[3] J. D. Lawson, *The Physics of Charged-Particle Beams* (Oxford Science, New York, 1988), and references therein.
[4] M. Reiser, *Theory and Design of Charged Particle Beams* (Wiley, New York, 1994).
[5] E. P. Lee and J. Hovingh, Fusion Tech. **15**, 369 (1989).
[6] R. W. Müller, in *Nuclear Fusion by Inertial Confinement: A Comprehensive Treatise*, edited by G. Velarde, Y. Ronen, and J. M. Martínez-Val (Chemical Rubber Co., Boca Raton, FL, 1993), Chap. 17, pp. 437–453.
[7] R. A. Jameson, in *Advanced Accelerator Concepts*, edited by J. S. Wurtele, AIP Conf. Proc. No. 279 (American Institute of Physics, New York, 1993), p. 969.
[8] R. Gluckstern, in *Oscillation Modes in Two-Dimensional Beams*, Proceedings of the 1970 Proton Linear Accelerator Conference, Batavia, IL, edited by M. R. Tracy (National Accelerator Laboratory, Batavia, IL, 1971), p. 811.
[9] R. C. Davidson, *Physics of Nonneutral Plasmas* (Ref. [1]), p. 699.
[10] H. Uhm and R. Davidson, Part. Accel. **11**, 65 (1980).
[11] I. Hofmann, L. Laslett, L. Smith, and I. Haber, Part. Accel. **13**, 145 (1983).
[12] J. Struckmeier and M. Reiser, Part. Accel. **14**, 227 (1984).
[13] J. Struckmeier, J. Klabunde, and M. Reiser, Part. Accel. **15**, 47 (1984).
[14] M. Tiefenback and D. Keefe, IEEE Trans. Nucl. Sci. **NS-32**, 2483 (1985).
[15] E. P. Lee, Nucl. Instrum. Methods Phys. Res. A **15**, 576 (1987).
[16] F. Guy, P. Lapostolle, and T. Wangler, in *The Influence of Density Distribution on the Stability Behavior of Beams*, Proceedings of the 1987 Particle Accelerator Conference, edited by E. R. Lindstrom and L. S. Taylor (IEEE, New York, 1987), p. 1149.

[17] C. Chen and R. C. Davidson, Phys. Rev. E **49**, 5679(1994).
[18] I. Kapchinskij and V. Vladimirskij, in *Proceedings of the International Conference on High Energy Accelerators and Instrumentation*, edited by L. Kowarski (CERN Scientific Information Service, Geneva, 1959), p. 274.
[19] H. Wiedemann, *Particle Accelerator Physics* (Springer-Verlag, New York, 1993).
[20] Q. Qian, Ph.D. thesis, Princeton University, 1995 (unpublished).
[21] R. C. Davidson and Q. Qian, Phys. Plasmas **1**, 3104 (1994).
[22] F. J. Sacherer, IEEE Trans. Nucl. Sci. **NS-18**, 1105 (1971).